https://doi.org/10.5194/essd-2026-432
Preprint. Discussion started: 11 August 2026

Open Access Earth System Science Data Discussions

A multi-band, multi-constellation shipborne GNSS dataset spanning a 216-day Antarctic circumnavigation

Blaž Bertalanič[1], Franc Dimc[2], and Aljaž Blatnik[3]

[1]SensorLab, Jožef Stefan Institute, Ljubljana, Slovenia
[2]Faculty of Maritime Studies and Transport, University of Ljubljana, Portorož, Slovenia
[3]Faculty of Electrical Engineering, University of Ljubljana, Ljubljana, Slovenia

Correspondence: Aljaž Blatnik (aljaz.blatnik@fe.uni-lj.si)

Abstract. We present a multi-band, multi-constellation Global Navigation Satellite System (GNSS) dataset comprising 216 daily files (two partial) recorded between 26 September 2025 and 29 April 2026 aboard the Italian research icebreaker R/V *Laura Bassi* during a round-trip voyage from Trieste to the Ross Sea sector of Antarctica and back, transiting the Panama Canal westbound on the outbound leg and Cape Horn (Drake Passage region) eastbound on the return. The route spans approximately 120° of geographic latitude (from 45.6° N to 74.8° S), includes eight crossings of the Antarctic Circle and two dwells in the Ross Sea. The instrument is a u-blox ZED-F9P-15B receiver paired with an NGS-calibrated Tersus AX4E02 multi-band geodetic-grade antenna, tracking GPS, GLONASS, Galileo, BeiDou, SBAS, QZSS and (where visible) NavIC across the L1 and L5 RF blocks. The release contains 37 144 455 high-precision navigation epochs and approximately 2.48 billion raw signal measurements at 2 Hz, together with approximately 18.6 million on-board radio-frequency spectrum messages (`UBX-MON-SPAN`, 1 Hz, one spectrum per RF block). On the basis of a structured literature and repository survey, we are not aware of a prior multi-month shipborne Antarctic GNSS dataset that preserves multi-band carrier-phase observables alongside dual-RF-block on-board `UBX-MON-SPAN` spectrum across both the L1 and L5 receiver blocks. Quality assessment finds a 3-D fix on every epoch after cold-start, 31.2 mean tracked satellites, code multipath of 0.4–1.0 m above 30° elevation, and best within-berth horizontal repeatability of 0.115 m at the Trieste return pier (cross-cluster median 0.57 m, $n = 10$ berths). Lyttelton (New Zealand) and its approaches account for nine of ten cruise-wide strong L-band RFI days. The deposit ships the raw binary `.ubx` alongside Hatanaka-compressed RINEX 3.04 (OBS+NAV) and the NGS-calibrated AX4E02 ATX. The open-source Python pipeline that produces the derived analyses referenced in this paper is bundled in the same Zenodo deposit under the MIT licence, with the development repository mirrored on GitHub. Use cases include kinematic positioning, tropospheric and precipitable-water-vapour retrieval, relative total-electron-content and rate-of-TEC products with a 2 Hz phase-scintillation proxy (with bandwidth caveats), and shipborne L-band radio-frequency interference surveillance. The complete dataset is openly available at https://doi.org/10.5281/zenodo.20344101 (Blatnik et al., 2026).

1 Introduction

Global Navigation Satellite Systems (GNSS) function not only as positioning instruments but as operational sensors for atmospheric water vapour, crustal deformation, ionospheric total-electron-content (TEC), and real-time space-weather indices

https://doi.org/10.5194/essd-2026-432
Preprint. Discussion started: 11 August 2026

Open Access Earth System Science Data Discussions

(Montenbruck et al., 2017; Jakowski et al., 2012). The International GNSS Service (IGS) Multi-GNSS Experiment (MGEX) (Montenbruck et al., 2017) anchors a network of geodetic-grade stations across continents, but its spatial sampling is intrinsically land-locked. The open ocean, and especially the Southern-Ocean ring south of 60° S, carries few permanent stations, producing a sampling gap in the same regions where polar-cap ionospheric activity, troposphere–ocean coupling, and L-band interference along major shipping corridors are most consequential. Three contemporaneous developments make closing this gap increasingly important. First, the L5/E5a/B2a civil band is increasingly available across GPS, Galileo and BeiDou, but multi-month shipborne records of the modernised civil signals at sea remain scarce. Second, publicly released ship-based records that preserve both the raw observables and the on-board RF spectrum are needed to characterise the rising prevalence of GNSS interference and spoofing in maritime environments. Third, the active phase of solar cycle 25 sustains elevated ionospheric activity through the 2024–2026 window (NOAA Space Weather Prediction Center, 2026), making fresh observations of polar-cap structure particularly informative. Multi-month, multi-band GNSS records on moving platforms remain the most direct way to close the gap (Bosser et al., 2021; Männel et al., 2021), but few publicly released examples exist, and none combine continuous multi-frequency raw observables with the on-board RF-spectrum diagnostics that modern receivers now stream natively.

Existing shipborne GNSS records typically lack one of three properties: multi-month duration, multi-band carrier-phase coverage, or on-board RF-spectrum preservation. EUREC4A (Bosser et al., 2021) and MOSAiC (Männel et al., 2021) are multi-month and multi-GNSS but focus on tropospheric water-vapour retrieval and do not preserve receiver-side spectrum. Our previous Italian Antarctic expedition (October 2024 – April 2025) released a 200-day single-frequency L1 record from the same vessel (Bertalanič et al., 2026), including L1-block `UBX-MON-SPAN` preserved at 1 Hz. That release demonstrated that a custom on-board logging chain can operate continuously through Antarctic conditions but left multi-band raw observables, dual-frequency ionospheric work, and the second (L5) RF block of the modernised civil-band receivers as open gaps. In the polar regions the gap is most acute: Antarctic terrestrial GNSS infrastructure (the West Antarctic GPS Network of Bevis et al. 2009 that grew into POLENET-Antarctica, the Italian and EUREF stations at Mario Zucchelli, Concordia and Rothera, and the SCAR-coordinated network) covers the continent well but does not sample the Southern-Ocean transit corridors, so polar ionospheric phenomena (high-latitude scintillation, polar-patch dynamics, total-electron-content irregularities) lack ground-track sampling between mid-latitudes and the Antarctic Peninsula (Alfonsi et al., 2011; Prikryl et al., 2015). GNSS-derived water-vapour products in the same region are similarly anchored to few fixed sites (Negusini et al., 2021).

Multi-band records of the on-board receiver RF spectrum (`UBX-MON-SPAN`) covering both the L1 and L5 receiver RF blocks from a moving platform are, to the best of our literature search, not currently available in open form. We surveyed the data-paper output of *Earth System Science Data*, *Scientific Data*, *Radio Science*, *GPS Solutions* and the *Journal of Geodesy* between 2019 and 2025, together with the PANGAEA, SEANOE and Zenodo repositories, using the keywords "UBX-MON-SPAN", "MON-SPAN", "GNSS spectrum monitoring" and "shipborne GNSS". Matches either covered single-band fixed-station deployments, short transects ($<$ 30 day), or our prior single-frequency MAX-M10S release (Bertalanič et al., 2026), which preserves `UBX-MON-SPAN` on the L1 RF block only. Multi-band shipborne campaigns (Bosser et al., 2021; Männel et al., 2021) preserve raw observables but not the receiver RF spectrum, while our prior single-frequency release (Bertalanič

https://doi.org/10.5194/essd-2026-432
Preprint. Discussion started: 11 August 2026

et al., 2026) preserves only the L1 RF block. The present dataset extends this lineage to continuous dual-RF-block (L1 and L5) on-board `UBX-MON-SPAN` alongside multi-band raw observables, building on the established use of u-blox `UBX-MON-SPAN` for L-band radio-frequency interference (RFI) surveillance and signal-quality monitoring (Morrison et al., 2019; Dovis, 2015).

Across 216 continuous days between 26 September 2025 and 29 April 2026, a u-blox ZED-F9P-15B multi-band GNSS module (firmware HPG L1L5 1.40) recorded aboard the Italian research vessel *Laura Bassi* (Polar Code PC5 Class A ice-breaker[1], operated by OGS) on a round-trip voyage between Trieste and the Ross Sea sector of Antarctica. The outbound leg ran westbound via the Mediterranean, the Atlantic, the Panama Canal and the Pacific to Lyttelton (NZ). The return leg ran eastbound from Lyttelton across the South Pacific, around Cape Horn (Drake Passage region) and up the Atlantic to Gibraltar and Trieste (Sect. 3 and Fig. 1). The route spans ≈120° of geographic latitude, both directions across the geomagnetic equator, and eight crossings of the Antarctic Circle (Table 1).

Table 1. Geographic-equator and Antarctic-Circle crossings during the cruise (UTC). The four main Antarctic-Circle crossings demarcate the two distinct Antarctic dwells. Four additional short-duration crossings on 14–16 February 2026 reflect the vessel operating within a few nautical miles of the 66.56° S parallel along longitudes 117–119° E.

Type	UTC time	Latitude	Longitude
Equator (S)	2025-11-01 18:44	0.000°	−86.433°
Antarctic Circle (S)	2025-12-02 21:23	−66.564°	−177.596°
Antarctic Circle (N)	2025-12-17 05:08	−66.564°	+176.692°
Antarctic Circle (S)	2026-01-06 22:57	−66.564°	+171.019°
Antarctic Circle (N)	2026-02-09 02:25	−66.564°	+164.631°
Antarctic Circle (S)	2026-02-14 01:54	−66.564°	+118.961°
Antarctic Circle (N)	2026-02-14 06:22	−66.564°	+117.751°
Antarctic Circle (S)	2026-02-16 07:32	−66.564°	+118.068°
Antarctic Circle (N)	2026-02-16 13:21	−66.564°	+117.009°
Equator (N)	2026-04-04 04:20	0.000°	−29.508°

The receiver tracks all four global navigation constellations (GPS, GLONASS, Galileo, BeiDou) plus regional SBAS, QZSS and (where visible) NavIC across the L1 and L5 frequency blocks at 2 Hz, alongside the 256-bin per-RF-block on-board RF spectrum (`UBX-MON-SPAN`, 1 Hz). Full receiver, antenna and recording-chain details are in Sect. 2.

The record opens four downstream directions in parallel: (i) kinematic positioning and code-multipath characterisation under varying sea state (Hamza et al., 2021); (ii) tropospheric and PWV retrieval via kinematic PPP with external precise orbit, clock and bias products (Bosser et al., 2021; Männel et al., 2021; Krietemeyer et al., 2020); (iii) ionospheric monitoring via per-arc geometry-free carrier-phase combinations feeding slant- and vertical-TEC analysis and the rate-of-TEC index (ROTI) (Pi et al., 1997; Jakowski et al., 2012); and (iv) L-band radio-frequency interference surveillance via the on-board RF spectrum

[1]The International Maritime Organization Polar Code class PC5 covers year-round operation in medium first-year ice that may include old ice inclusions.

https://doi.org/10.5194/essd-2026-432
Preprint. Discussion started: 11 August 2026

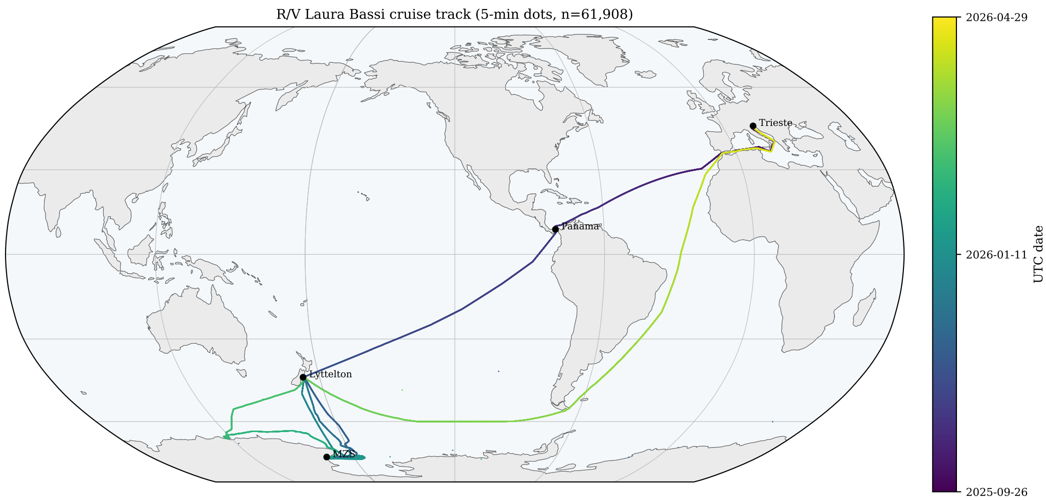

Figure 1. Cruise track of R/V *Laura Bassi*, 26 September 2025 to 29 April 2026 (216 days), as recorded by the on-board ZED-F9P-15B receiver paired with the Tersus AX4E02 antenna. The track is rendered as a scatter point cloud (one decimated 5-min mean position per dot, ≈62 000 dots, coloured by UTC date from cool to warm) because a continuous polyline would jump across the antimeridian for the Pacific transit and across daily log-rotation gaps. The time ordering can be read directly from the colour gradient. The Pacific-centred Robinson projection is chosen so the Atlantic–Pacific–Indian–Atlantic loop reads as a single closed curve. Trieste (departure/return), Panama Canal, Lyttelton (Antarctic-staging port) and Mario Zucchelli station are marked.

(`UBX-MON-SPAN`) and jamming-indicator diagnostics (`UBX-MON-RF`) (Borio and Gioia, 2015; Morrison et al., 2019; Dovis, 2015). For ionospheric work we publish a 2 Hz σ_φ-equivalent proxy and the ROTI field with explicit bandwidth caveats, and release vertical-TEC products as relative quantities. The quality-control pass identifies one notable finding: Lyttelton (NZ) and its approaches are a strong L-band RFI hotspot, accounting for nine of ten cruise-wide strong-RFI days (Sect. 5). The present paper is restricted to data description and quality assessment.

The data archive ships the original binary `.ubx` logs (preserving the on-board `UBX-MON-SPAN` RF spectrum and all u-blox diagnostics) and the derived RINEX 3.04 set (Hatanaka-compressed OBS+NAV) as the two primary source formats, plus the NGS-calibrated AX4E02 ATX, an IGS-style site log, a deposit `README` and SHA-256 checksums. The open-source Snakemake pipeline used to produce the analyses, tables and figures in this paper is bundled in the same Zenodo deposit under the MIT licence (Sect. 10). The remainder of this paper is organised as follows. Section 2 describes the receiver, antenna, mounting and on-board recording chain. Section 3 documents the cruise itinerary and daily-file conventions. Section 4 details the processing pipeline. Section 5 reports quality-control statistics and the external positional-validation exercise across the 216 days. Section 6 collects the dataset's intended-use caveats and known limitations. Section 7 describes the data records and deposit structure. Section 8 positions the dataset against prior openly-released shipborne GNSS campaigns. Sections 10 and 11 give code and data availability.

https://doi.org/10.5194/essd-2026-432
Preprint. Discussion started: 11 August 2026

2 Instrumentation

2.1 GNSS receiver

The recording instrument is a u-blox ZED-F9P-15B high-precision GNSS module (u-blox AG, 2024) running firmware HPG L1L5 1.40 (Table 2 summarises the full configuration). The F9P is a dual-band, multi-constellation receiver with a two-channel RF front-end (L1 and L5) and concurrent tracking of GPS, GLONASS, Galileo, BeiDou, SBAS, QZSS, and NavIC (where visible). Independent validation studies report centimetre-level real-time-kinematic accuracy with appropriate antennas (Hamza et al., 2021; Krietemeyer et al., 2020) and demonstrate that its raw observables are competitive with geodetic-grade equipment for tropospheric, ionospheric, and PPP-AR work (Hamza et al., 2021; Poluzzi et al., 2020).

Table 2. Receiver, antenna and recording-chain configuration.

Parameter	Value
Receiver manufacturer	u-blox
Receiver model	ZED-F9P-15B
Firmware	HPG L1L5 1.40
Antenna manufacturer	Tersus GNSS
Antenna model	AX4E02
Antenna calibration	NGS-calibrated (NOAA National Geodetic Survey, 2026)
Cable	10 m RG223, UV- and water-protected
RINEX marker name / type	`JSI1` / `NON_GEODETIC` (with `MOVING` comment)
Recording rate (NAV/RAWX)	2 Hz
Recording rate (`UBX-MON-SPAN`)	1 Hz
RF bands monitored	Upper Band (L1 / E1 / B1); 1559–1606 MHz
	Lower Band (L5 / E5a / B2a); 1166–1188 MHz
Constellations tracked	GPS, GLONASS, Galileo, BeiDou, SBAS, QZSS, NavIC

The HPG L1/L5 firmware variant tracks the L1 band on every constellation and the L5 band on the L5-family signals only: GPS L5 (broadcast by Block IIF and Block III satellites, approximately half of the operational GPS constellation), Galileo E5a, BeiDou B2a, QZSS L5 and NavIC L5. It does not track GLONASS L2OF, GPS L2C/P, Galileo E5b/E6 or BeiDou B2I/B3I. Consequently the dataset is dual-band for GPS Block IIF/III, Galileo, BeiDou and QZSS (when L5 is broadcast), and single-band (L1 only) for GLONASS, SBAS, legacy GPS Block IIR/IIR-M, and intermittently for QZSS. NavIC, which is broadcast on L5 only, is single-band by design. This coverage profile shapes the geometry available to downstream dual-frequency products such as kinematic PPP and ionospheric-combination work (Sect. 5).

We refer to the receiver's second RF passband as the "L5 RF block" throughout this paper. u-blox's hardware designation for the same passband is "L2/L5" because it is 128 MHz wide and centred at 1191.5 MHz, physically receiving both

https://doi.org/10.5194/essd-2026-432
Preprint. Discussion started: 11 August 2026

Figure 2. Mounted antenna on the Laura Bassi ship.

the L5 frequency family (near 1176.5 MHz: GPS L5, Galileo E5a, BeiDou B2a, QZSS L5, NavIC L5) and the L2 frequency family (1207–1248 MHz: BeiDou B2I, Galileo E5b, GPS L2C/P, GLONASS L2OF). The HPG L1/L5 firmware variant configures this block to correlate only the L5-family signals, so all positioning observables are L5-band. The captured spectrum (`UBX-MON-SPAN`) and the per-block jamming indicator (`UBX-MON-RF.jamInd`) nevertheless report RF energy across the full 128 MHz passband and therefore observe L2-band interference too, even though no L2 signal enters the positioning solution.

2.2 Recorded message streams

All on-board observables and diagnostics are streamed in u-blox's proprietary UBX binary protocol (u-blox AG, 2024). Message names below follow the u-blox `UBX-<class>-<id>` convention used throughout this paper and are distinct from the RINEX 3.04 redistribution described in Sect. 4. With the receiver operated in its default high-precision mode, nine UBX message streams are recorded continuously throughout the cruise (Table 3): three navigation-solution streams, three raw-measurement streams, and three receiver-diagnostic streams.

2.3 Antenna

The receiver was paired with a Tersus AX4E02 (Figure 2) full-constellation survey antenna (Tersus GNSS Inc., 2024): an NGS-calibrated, multi-band, RHCP-polarised antenna with a datasheet vertical (Up-axis) L1 phase-centre offset of 59.14 mm and a published phase-centre accuracy of ±2 mm; the full per-frequency PCO/PCV is provided in the bundled NGS-calibrated ATX file (Sect. 7). Frequency coverage spans GPS L1/L2/L5, GLONASS L1/L2/L3, BeiDou B1/B2/B3, Galileo E1/E5a/E5b/E6, QZSS L1/L2/L5/L6, NavIC L5, SBAS L1/L5 and the L-band correction service. Datasheet figures include LNA gain 40 dB

https://doi.org/10.5194/essd-2026-432
Preprint. Discussion started: 11 August 2026

Table 3. u-blox UBX message streams recorded continuously throughout the cruise. Each row gives the message name (following the u-blox UBX-<class>-<id> convention), its emission rate, and a one-line description of the contents. The parsed Parquet column schemas used in this paper are documented in the released codebase (Sect. 10).

Message	Rate	What it reports
Navigation solution		
UBX-NAV-PVT	2 Hz	Kalman-filtered position/velocity/time fix with fixType, numSV, ground speed, formal-error hAcc/vAcc
UBX-NAV-HPPOSLLH	2 Hz	High-precision lat/lon/height (0.1 mm resolution) emitted at the same epoch as UBX-NAV-PVT
UBX-NAV-SAT	2 Hz	Per-satellite elevation, azimuth, C/N_0 and used-in-solution flag for every tracked SV
Raw measurements		
UBX-RXM-RAWX	2 Hz	Multi-band raw observables: pseudorange, carrier phase, Doppler, C/N_0, lock-time and tracking status per signal
UBX-RXM-MEASX	2 Hz	Pre-PVT multi-band measurements used internally for code-pseudorange smoothing
UBX-RXM-SFRBX	on subframe	Broadcast navigation subframes per signal (ephemeris, almanac and ionosphere model source for self-contained PPP and reproducibility)
Receiver diagnostics		
UBX-MON-RF	1 Hz	Per-RF-block jamming indicator, AGC count, noise-per-ms and antenna power state
UBX-MON-SPAN	1 Hz	256-bin on-board RF spectrum per RF block (L1 block centred at 1583.5 MHz; L5 block centred at 1191.5 MHz; both with 128 MHz span, ≈500 kHz/bin)
UBX-MON-SYS	≈0.5 Hz	CPU load, memory, runtime and uncalibrated receiver-internal temperature telemetry

(typical), noise figure ≤ 2 dB, peak gain ≤ 5.5 dBi, axial ratio ≤ 3 dB and group delay ripple < 5 ns. An internal multipath-rejection board is fitted, the unit is IP67-rated and rated for $-40\,°$C to $+85\,°$C ambient. The published NGS calibration ANTEX file (marker TRSAX4E02, radome NONE) is available from the NGS antenna calibration database (NOAA National Geodetic Survey, 2026). Users reprocessing the RINEX archive with PRIDE PPP-AR or comparable software should merge this entry into their processor's IGS20 ATX catalogue, after which receiver-side PCO/PCV corrections are applied automatically. Without the merge the corrections silently default to zero.

https://doi.org/10.5194/essd-2026-432
Preprint. Discussion started: 11 August 2026

Open Access Earth System Science Data Discussions

2.4 Mounting and recording chain

The antenna was mounted on the upper deck of R/V *Laura Bassi* (PC5 Class A icebreaker, operated by OGS) with a clear sky view in all azimuths. A 10 m RG223 coaxial cable with additional UV and water protection connects the antenna to the receiver, which is housed inside an IP65 enclosure in the ship's communications cabin above the bridge. Mains-derived 3.3-V DC powers the antenna LNA via the receiver's `VCC_RF` line. Short-circuit and lightning-protection circuits on both ends of the cable protect the chain against transient events (Tersus GNSS Inc., 2024).

A custom-built multi-SD-card logger streams the binary `.ubx` data from the F9P's UART interface in real time, with file rotation at 00:00 UTC each day. The full list of recorded UBX sentences and their sampling frequencies can be seen in Table 3.

2.5 Time reference

The receiver derives its time tag from the GPS satellites' broadcast time, with a leap-second offset of 18 s applied to convert to UTC. The `UBX-NAV-PVT` message reports both the iTOW (week-relative GPS time) and the UTC year/month/day/hour/min/sec/nano fields. All datasets in the released archive use UTC throughout.

3 Data acquisition

3.1 Cruise itinerary

The acquisition campaign covered the full operational cycle of *Laura Bassi* between two consecutive Italian polar missions (Fig. 1). The vessel departed Trieste, Italy (45.6131° N, 13.8092° E) on 2025-09-26 and returned to the same port on 2026-04-29, tracing a closed-loop round-trip voyage. The outbound leg ran westbound: Mediterranean, Atlantic, Panama Canal, and mid-Pacific transit to the Antarctic-staging port of Lyttelton (New Zealand). Two Antarctic dwells in the Ross Sea sector followed, with Mario Zucchelli station as the principal anchorage and brief operations along the East Antarctic margin at 117–119° E in mid-February 2026. The return leg ran eastbound: from Lyttelton across the South Pacific, around Cape Horn (Drake Passage region), north through the South and North Atlantic, through the Strait of Gibraltar, and through the western Mediterranean back to Trieste. The cruise traversed ≈120° of geographic latitude (from 45.6° N to 74.8° S) and crossed the Antarctic Circle eight times: four main north/south crossings demarcate the two Antarctic dwells, plus four short-duration boundary oscillations on 14–16 February 2026 along longitudes 117–119° E. Precise UTC times and coordinates for the equator and Antarctic-Circle crossings are tabulated in Table 1.

3.2 Recording schedule and file convention

Logging was continuous at 2 Hz for the navigation and raw-observable streams and at 1 Hz for the diagnostic streams (Sect. 2.2). The 2 Hz rate is preserved from our prior expedition (Bertalanič et al., 2026) and is sub-samplable to 1 Hz for direct comparability with the multi-month shipborne records of Bosser et al. (2021); Männel et al. (2021). The 1 Hz Nyquist limit this implies for the ionospheric scintillation product is documented as a caveat in Sect. 6.

https://doi.org/10.5194/essd-2026-432
Preprint. Discussion started: 11 August 2026

The on-board logger rotated files at 00:00 UTC each day, producing one binary `.ubx` file per UTC date named `YYYYMMDD.ubx`. Two files are partial: `20250926.ubx` (∼15.4 h, starting at 08:35 UTC after receiver power-up at the dock) and `20260429.ubx` (∼7.8 h, ending on return arrival). The remaining 214 files cover a full 24-hour UTC day. Total recorded volume is 176.9 GB across the 216 files (mean 819 MB, range 253 MB–887 MB).

3.3 Receiver state and uptime

The receiver held a three-dimensional fix on every epoch after the initial cold start (the first 9 epochs of 2025-09-26, ≈ 4.5 s at 2 Hz, carry a 2-D fix). No firmware updates or hardware interventions were performed during the cruise. The `UBX-MON-VER` caveat on firmware-string provenance is discussed in Sect. 6.

4 Data processing

4.1 Pipeline overview

All derived products are reproducible from the raw `.ubx` archive through a Snakemake-orchestrated, day-parallel pipeline released alongside this paper (Sect. 10). The pipeline parses the binary stream into per-message Apache Parquet tables and a `UBX-MON-SPAN` Zarr v3 store, derives the cruise-track, multipath, TEC and scintillation-proxy products described below, rolls per-day artefacts into the cruise-wide quality summary tables, renders all figures, and finally produces the RINEX 3.04 OBS+NAV archive (`convbin` from the RTKLIB demo5 fork (Everett, 2024), Hatanaka-compressed). Reproducibility is bit-for-bit for the binary-decode, derived-analysis and figure stages; the kinematic PPP-AR pass (Sect. 5) is deterministic to within ambiguity-resolution tolerances of the external processor, so PPP residuals at the centimetre-to-decimetre level may differ between rebuilds with the same external products.

4.2 Binary parser

A custom Python decoder produces per-message Apache Parquet tables and a Zarr v3 store from the raw `.ubx` stream via the released pipeline (Sect. 10). Inter-frame Fletcher-8 checksums are recomputed. The cruise-wide rate of checksum-rejected frames is 4.7×10^{-7} (2 066 of 4.4×10^{9}), making the framing channel effectively lossless.

4.3 Data products

4.3.1 Per-message Parquet and `UBX-MON-SPAN` Zarr

Eight message types are decoded to long-form, compressed Apache Parquet (`nav_pvt`, `nav_hpposllh`, `nav_sat`, `rxm_rawx`, `rxm_sfrbx`, `rxm_measx`, `mon_rf`, `mon_sys`). The on-board RF spectrum (`UBX-MON-SPAN`) is preserved separately in a Zarr v3 store indexed by (time, RF block, frequency bin).

https://doi.org/10.5194/essd-2026-432
Preprint. Discussion started: 11 August 2026

4.3.2 Cruise track

The cruise trajectory is built from `nav_hpposllh` high-precision positions filtered against a single set of outlier criteria (low fix quality, out-of-cruise timestamps, null-island sentinels, implausible horizontal accuracy, and physically impossible inter-fix speeds; exact thresholds documented in the released pipeline). The pipeline emits the clean track in Parquet (per-day and aggregate), GeoJSON and CF-compliant NetCDF for downstream use.

4.3.3 Code-multipath, ROTI and scintillation proxy

The Estey & Meertens M1 and M2 code-multipath linear combinations (Estey and Meertens, 1999) are computed per-arc and per-elevation bin from the F9P's dual-band signal pairs (GPS L1+L5, Galileo E1+E5a, BeiDou B1I+B2a) after per-arc bias removal. The same arc-segmenter feeds the geometry-free carrier-phase combinations used to derive slant TEC and rate-of-TEC (ROTI, computed over rolling 300 s windows). A phase-detrended σ_φ proxy at 2 Hz is computed by 60 s polynomial detrending of the carrier phase. The canonical amplitude index S_4 is not derivable at 2 Hz. The σ_φ proxy's 1 Hz Nyquist limits sensitivity to scintillation power above ≈ 0.5 Hz and downstream users should treat it as a lower bound at high-latitude sites.

4.3.4 Anomaly catalogue and spoofing detection

A separate module flags every per-day epoch whose fix-type / position / time / RF state exceeds a defined threshold and records the result in a per-day anomaly catalogue. The catalogue distinguishes the seven categories listed in Table 4 (high-jamming flags are kept separate per RF block because the L5 baseline is a known receiver-internal effect rather than environmental RFI, see Sect. 5). Every flagged row carries the full local context required to interpret it: position, fix type, number of SVs in solution, horizontal accuracy, distance and implied speed to the previous good fix, plus the jamming indicator and AGC count from `UBX-MON-RF` on both RF blocks at the same epoch.

A complementary multi-signature spoofing detector combines the seven independent indicators listed in Table 5 into a per-epoch suspicion score on $[0,7]$. Each indicator is clamped to $[0,1]$ at the tabulated saturation threshold and the seven clamped contributions are summed; full numeric clamping logic is in the `anomaly` module of the released pipeline (Sect. 10). Output lands in a per-day spoofing catalogue. Cruise-wide results are reported in Sect. 5. Flagged epochs remain in the released archive; the anomaly and spoofing catalogues are diagnostic overlays only.

4.4 RINEX 3.04 archive

A complementary RINEX 3.04 OBS+NAV release is produced from the demo5 RTKLIB fork (Everett, 2024), which correctly maps the ZED-F9P-15B's signal-id allocation to the RINEX 3 observation codes. Per-constellation observation-type sets follow the L1L5 firmware coverage described in Sect. 2 and are listed in the deposit `README`. Broadcast navigation messages (ephemerides, almanac and ionosphere-model coefficients) are extracted from the `UBX-RXM-SFRBX` subframe stream and written into the per-day RINEX 3.04 NAV files, so users do not need to fetch external broadcast products to reprocess any

https://doi.org/10.5194/essd-2026-432
Preprint. Discussion started: 11 August 2026

Table 4. Anomaly catalogue categories. Every per-epoch flag is preserved in the per-day anomaly catalogue together with local context (lat/lon, fix type, numSV, hAcc/vAcc, `UBX-MON-RF.jamInd` and `UBX-MON-RF.agcCnt` on both RF blocks, distance and implied speed to the previous good fix).

Category	Definition
`boot_state`	Receiver clock outside the cruise window ($t_{ns} <$ 2025-01-01 or $>$ 2027-01-01). Typically pre-fix epochs in the receiver cold-start sequence.
`no_fix`	`fixType` < 3 (no 3-D solution). Reported coordinates may be cached values from a previous lock.
`null_island`	Reported `lat` = `lon` = 0. A receiver-side sentinel that appears occasionally during fix re-acquisition.
`speed_outlier`	Implied great-circle speed from the previous good fix exceeds 100 kt, which no surface vessel can produce.
`possible_spoof`	`speed_outlier` *and* `fixType` ≥ 3 *and* `hAcc` < 5 m *and* both `UBX-MON-RF` blocks report nominal `jamInd`. The receiver reporting an apparently-clean, high-accuracy jump is the canonical spoofing fingerprint.
`high_jamming_l1`	`UBX-MON-RF.jamInd` above a per-day threshold on the L1 block, defined as $\min(60,\ \max(\text{median} + 5\,\text{MAD},\ 40))$ over that day's L1 `jamInd` samples. The absolute floor of 60 captures loud events regardless of baseline; the relative term $\text{median} + 5\,\text{MAD}$ catches context-relative excursions on otherwise-quiet days, clamped at a per-day minimum of 40 (just above the 17–30 sea-going baseline) so the discrete `jamInd` distribution does not flag its own baseline. Merged with the row even when no other category applies.
`high_jamming_l5`	`UBX-MON-RF.jamInd` above the analogous per-day threshold on the L5 block, $\min(130,\ \max(\text{median} + 5\,\text{MAD},\ 110))$ (the L5 baseline is 70–100). Merged with the row even when no other category applies.

single day. RINEX files use the long IGS file-naming convention, are Hatanaka-compressed and gzipped. The `MARKER TYPE` is set to `NON_GEODETIC` with a `MOVING` comment to indicate the moving platform.

Because RINEX 3.04 has no formal field for time-varying antenna coordinates, an a-priori cruise trajectory generated by the released pipeline from `UBX-NAV-HPPOSLLH` (Sect. 10) must be supplied to PRIDE PPP-AR (Geng et al., 2024) or similar processors. The antenna ARP-to-marker offset is zero by construction (`ANTENNA: DELTA H/E/N` $= (0,0,0)$ in

https://doi.org/10.5194/essd-2026-432
Preprint. Discussion started: 11 August 2026

Open Access Earth System Science Data Discussions

Table 5. Seven indicators combined into the per-epoch spoofing suspicion score $S \in [0, 7]$ (one per row, each clamped to $[0, 1]$). The numeric threshold tabulated for each indicator is the value at which the indicator's contribution saturates at 1.0. All thresholds are documented in the released pipeline (Sect. 10). Persistent $S \geq 3$ warrants visual inspection. $S \geq 5$ is a strong flag. None of the 216 cruise days reaches $S \geq 5$ on any epoch (Sect. 5).

Indicator (saturation threshold)	Rationale
`agc_drop` (AGC drop $> 2\sigma$, daily)	AGC falls without the jamming indicator rising, the signature of an injected signal stronger than real GNSS.
`cno_uniformity` (per-epoch C/N$_0$ std < 12 dB-Hz)	Single-antenna spoofers produce near-uniform C/N$_0$ across the injected constellation.
`cno_elev_slope` (slope magnitude < 0.15 dB-Hz per $^\circ$)	Real broadcasts show a ∼1.5–2 dB-Hz per 10° elevation trend, which spoofers flatten.
`constellation_inconsistency` (per-GNSS prRes std > 10 m)	A single spoofer rarely targets all GNSS coherently.
`pos_vel_mismatch` (haversine vs `gSpeed`, normalised by speed)	Fixed-position spoofs produce stationary coordinates with nonzero reported velocity.
`time_jump` (non-monotonic `iTOW`)	Receiver clock retreats or stalls between consecutive `UBX-NAV-PVT` epochs.
`hp_pvt_div` (3-D `UBX-NAV-HPPOSLLH` − `UBX-NAV-PVT` > 0.5 m)	The two filter chains diverge during spoofing transients.

every header), so the marker tracks the antenna phase centre directly; the antenna's absolute height above the ship's nominal reference point (waterline or hull reference) is not corrected here and is documented in the IGS-style site log (Sect. 7). The NGS-calibrated AX4E02 PCO/PCV correction is shipped under `rinex3/antex/` for users to merge into their processor's IGS20 ATX catalogue (Sect. 6).

5 Quality control and uncertainty

We assess data quality along eight independent axes: (1) receiver internal consistency from the two on-board position solutions; (2) fix availability and constellation tracking across the cruise; (3) external positional validation by within-berth repeatability and an independent kinematic-PPP cross-check; (4) a continuous consistency check against the ship's primary L1-only navigation receiver; (5) code multipath and cycle-slip statistics; (6) ionospheric product cross-validation against the IGS Global Ionosphere Map; (7) RF spectrum baseline and the strong-RFI event catalogue; and (8) track-outlier classification. Each subsection below states the method and reports the cruise-wide result. Limitations and intended-use caveats are collected in Sect. 6.

5.1 Receiver internal consistency

The receiver emits two independent position solutions per epoch: a Kalman-filtered `UBX-NAV-PVT` fix and a direct high-precision `UBX-NAV-HPPOSLLH` fix. The median 2-D horizontal distance between the two solutions is 4 mm (95th percentile

https://doi.org/10.5194/essd-2026-432
Preprint. Discussion started: 11 August 2026

6 mm), the median vertical difference is 0.3 mm (95th percentile 0.5 mm), and the maximum 2-D distance on any single epoch is below 0.05 m. We did not detect a systematic dependence of these figures on latitude or on day-mean ground speed.

5.2 Fix availability and constellation tracking

The dataset comprises 37 144 455 `UBX-NAV-PVT` epochs. The mean number of satellites in the navigation solution per epoch is 31.2, ranging from a daily mean of 27.0 on 2026-03-30 (South Atlantic transit, on the return leg) to 31.8 on 2025-11-01 (Atlantic transit, near the geomagnetic equator). Position dilution of precision (pDOP) averages 0.98. No day has a daily mean exceeding 2.0. A 3-D fix is held on every epoch except for the 9 cold-start epochs on 2025-09-26.

The raw measurements (`UBX-RXM-RAWX`) total approximately 2.48 billion individual signal observations, broken down per (GNSS, sigId) in Table 6. GLONASS L1 OF carries the highest mean C/N_0 (46.3 dB-Hz), consistent with the stronger broadcast level of its FDMA signals relative to the CDMA counterparts. NavIC L5 (`gnssId` = 7) is retained despite the IRNSS constellation's nominal coverage being centred on the Indian Ocean: the receiver tracked NavIC GEO satellites at non-trivial C/N_0 across both the Indian-Ocean and Antarctic legs.

Table 6. Constellation/signal coverage across 216 days. Total observation counts and mean carrier-to-noise-density ratio (C/N_0) per (GNSS, signal) pair from `UBX-RXM-RAWX`. Signal labels follow the u-blox `(gnssId, sigId)` convention parsed from the binary stream; the QZSS L5 row corresponds to `sigId` = 9 (pilot component Q).

GNSS	Signal	N obs (M)	Mean C/N_0 (dB-Hz)
GPS	L1 C/A	331	42.4
GPS	L5 Q	209	45.7
GLONASS	L1 OF	331	46.3
Galileo	E1 C	320	41.5
Galileo	E5a I	322	43.3
BeiDou	B1I D1	475	43.4
BeiDou	B2a Q	345	43.8
SBAS	L1	65	39.5
QZSS	L1 C/A	22	36.7
QZSS	L5 Q	14	44.4
NavIC	L5	42	32.7
Total		2476	

5.3 External positional validation

Validating a moving-platform receiver against an independent reference is non-trivial because no continuous ground truth exists along the track. We adopt a two-pronged approach: a *within-berth repeatability* metric whenever the ship is stationary, and a

https://doi.org/10.5194/essd-2026-432
Preprint. Discussion started: 11 August 2026

kinematic post-processing PPP solution as an external precision benchmark across the full cruise. The within-berth metric exploits the fact that each time the ship returns to the same physical mooring, the median position fix during a stationary window (ground speed $< 0.1\,\mathrm{m\,s^{-1}}$ for at least 30 min; multiple such windows can occur within a single port stop) should remain constant to within the receiver's positioning uncertainty.

The ship occupied 10 distinct physical berths, each contributing at least three stationary windows (one window = one ≥ 30 min quiescent period at < 0.1 m/s; a single port stop typically contributes several such windows). Distinct berths within the same harbour are resolved by greedy 50-metre sub-clustering on the per-window median position (Fig. 3). The Trieste return pier ($n = 10$ windows) yields the best within-berth horizontal repeatability at 0.115 m, the Trieste departure pier ($n = 11$ windows) 0.243 m, the Lyttelton sub-berths ($n = 3$–16, six clusters) 0.51–0.67 m, and the Mario Zucchelli anchorage ($n = 20$ windows) 1.24 m, the worst of the tight clusters and consistent with sea-state-induced antenna motion at anchor. One Lyttelton cluster ($n = 15$, $\sigma = 7.22$ m, ≈ 1.2 km offset from the main sub-berth area) is excluded as a wider anchorage zone artificially bundled by the 50 m cutoff. The cross-berth median across all 10 clusters is 0.57 m. These figures are consistent with published F9P benchmarks (Hamza et al., 2021) and span the decimetre-to-metre range of at-berth horizontal repeatability across the three port and anchorage regions sampled (best 0.115 m at Trieste; worst 1.24 m at Mario Zucchelli).

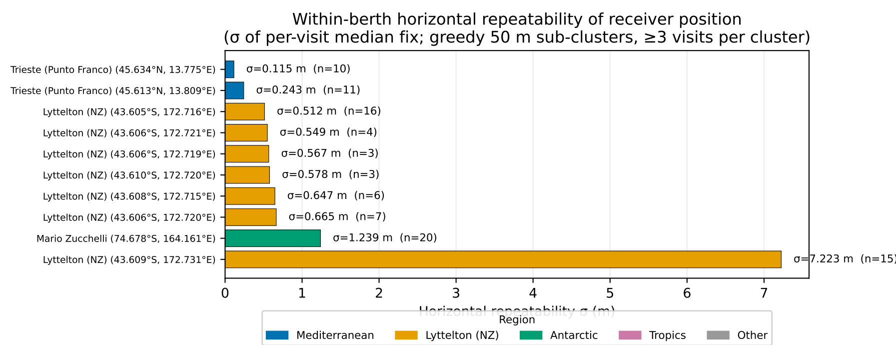

Figure 3. Within-berth horizontal repeatability of the receiver position. For each of the 10 physical berths revisited on at least three stationary windows (n values shown on the right of each bar), the bar height is the standard deviation of the per-visit median position, computed in metres around the berth-mean using the local Earth radius. The Trieste return pier ($n = 10$) is the best at 0.115 m. The Mario Zucchelli anchorage ($n = 20$) is the worst of the tight clusters at 1.24 m, consistent with sea-state-induced antenna heave at anchor. The cross-berth median (across the 10 clusters) is 0.57 m. One Lyttelton cluster ($n = 15$, $\sigma = 7.22$ m) is shown at the bottom of the panel. We attribute it to a wider anchorage zone bundled into a single greedy-50 m cluster rather than to receiver repeatability, and exclude it from the cross-berth maximum statistic in the body text.

The distribution of position-quality metrics across all 37 144 455 `UBX-NAV-PVT` epochs is reported in Table 7. We distinguish two metrics: the receiver-internal Kalman-filter *formal error* (`UBX-NAV-HPPOSLLH.hAcc` and `vAcc`) which represents the filter's self-reported precision, and the *difference* between the onboard fix and an independent kinematic PPP solution (PRIDE PPP-AR, `pdp3 -m K`, Wuhan multi-GNSS rapid orbit, clock, attitude, ERP and code/phase-bias products (Wuhan

https://doi.org/10.5194/essd-2026-432
Preprint. Discussion started: 11 August 2026

University IGS Analysis Center, 2024), ambiguity resolution enabled) which represents external accuracy. The PPP solution anchors the moving F9P record to the IGS reference frame (IGS20, aligned with ITRF2020) via the WUM orbit, clock, attitude, ERP and observable-specific bias products (Wuhan University IGS Analysis Center, 2024; Geng et al., 2022), themselves derived from the global network of geodetic-grade IGS reference stations. The onboard-vs-PPP residual therefore serves as the dataset's precision benchmark against the IGS reference frame, computed without dependence on any single nearby ground station. The two metrics are not the same: the formal error excludes unmodelled multipath, antenna phase-centre and troposphere-model error, and is known to be optimistic for consumer-grade multi-band receivers on moving platforms (Hamza et al., 2021).

Across the 216-day cruise the onboard horizontal formal error (`hAcc`) is 0.32 m at the median and 0.55 m at the 95th percentile (Table 7, $n = 37.1$ million epochs). The median onboard-vs-PPP 3-D residual across the PPP-covered subset is 2.96 m ($p_{95} = 8.37$ m, $p_{99} = 13.96$ m; Table 7, $n = 14.2$ million matched epochs spanning 188 of the 216 cruise days). PPP coverage excludes 28 days: five scattered days where the kinematic solution failed to converge to the standard tolerances (2026-01-01, 2026-03-02, 2026-03-03, 2026-03-06, 2026-03-28), and 23 of the closing 27 cruise days (within 2026-04-03 to 2026-04-29) for which the orbit, clock and bias products required by PRIDE PPP-AR were not yet released at the time the dataset was finalised (the WUM rapid products PRIDE selected for the rest of the cruise are released with a multi-day latency, and IGS final products with a multi-week latency). These exclusions are operational rather than geographic; they do not oversample any one cruise leg. We intend to extend the kinematic-PPP cross-check to these closing days once the corresponding IGS final products become available, and to release the updated residuals as a versioned revision of the Zenodo deposit under the ESSD living-data process. The residual budget is dominated by harbour multipath (Trieste, Lyttelton, Mario Zucchelli anchorages), partial dual-frequency geometry under the L1L5 firmware variant (Sect. 2: dual-band ionosphere-free combinations form only for Galileo E1+E5a, BeiDou B1I+B2a, GPS L1+L5 on Block IIF/III, and QZSS L1+L5 when broadcast; GLONASS, SBAS, legacy GPS and intermittent QZSS contribute as single-frequency observations), residual antenna phase-centre error, and tropospheric-model mismatch over the marine boundary layer. We publish the onboard fix as the practical primary trajectory because it is continuous, free of PPP convergence transients, and independent of post-mission precise-product availability. The PPP solution serves as the independent cross-check against which the onboard track is validated in this paper: the PPP-covered-subset percentiles of the PPP-vs-onboard residual in Table 7 are the headline validation result and define the realistic position-uncertainty envelope downstream products inherit.

PPP reprocessing uses a frequency-combination string (`G15 E15 C25 J15`) matched to the L1L5 firmware variant, applies the NGS-calibrated AX4E02 PCO/PCV correction (Sect. 6), and forms dual-frequency ionosphere-free combinations for GPS Block IIF/III, Galileo, BeiDou and intermittent QZSS. GLONASS contributes code-only.

https://doi.org/10.5194/essd-2026-432
Preprint. Discussion started: 11 August 2026

Open Access Earth System Science Data Discussions

Table 7. Distribution of position formal errors and PPP-vs-onboard residuals across the 216-day cruise. Each row reports the percentiles p_1, p_5, p_{10}, p_{50}, p_{90}, p_{95}, p_{99} in metres, with n the number of contributing epochs. Following the format of Bosser et al. (2021) Table 3. The onboard rows are the receiver's Kalman-filter self-reported `hAcc` and `vAcc` formal errors aggregated over every `UBX-NAV-HPPOSLLH` epoch in the cruise. The PPP rows aggregate the per-epoch onboard-vs-PRIDE PPP-AR horizontal, vertical and 3-D residuals over the kinematic reprocessing pass described in Sect. 5 ($n = 14{,}155{,}091$ matched epochs from the days for which PPP has converged).

Metric	p_1	p_5	p_{10}	p_{50}	p_{90}	p_{95}	p_{99}	n
Onboard `hAcc` (m)	0.22	0.24	0.26	0.32	0.51	0.55	0.63	37 144 455
Onboard `vAcc` (m)	0.33	0.36	0.39	0.56	0.80	0.88	0.99	37 144 455
PPP horiz. residual (m)	0.15	0.35	0.51	1.62	4.43	6.10	11.47	14 155 091
PPP vert. residual (m)	0.03	0.15	0.29	1.68	5.02	6.34	9.95	14 155 091
PPP 3-D residual (m)	0.43	0.79	1.07	2.96	6.41	8.37	13.96	14 155 091

5.4 Cross-receiver consistency check against the ship's navigation suite

The F9P-derived cruise track is additionally cross-checked against the ship's own primary GPS, broadcast at ≈ 12-minute cadence on the OGS near-real-time dashboard[2]. This is a *consistency* check, not a precision benchmark: neither the F9P nor the OGS feed has independent ground truth, so the comparison cannot establish which receiver is more accurate. What it can show is whether the F9P exhibits position anomalies that its own internal-consistency and berth-repeatability checks (Sect. 5, above) would miss. This is a useful guard given that the OGS feed runs on a sensor chain, antenna mount and operating crew entirely independent of the F9P + AX4E02 acquisition.

For each OGS timestamp we take the nearest F9P sample (median match-gap 0.5 s) and compute the haversine horizontal residual. The two OGS campaigns available at submission time cover 149 of 216 cruise days ($n = 18105$ matched fixes). During port-dwell windows (ship ground speed below 0.2 m/s, $n = 4569$ fixes) the median F9P–OGS residual is 5.16 m ($p_{90} = 7.21$ m). The moving-fix subset is consistent with the same picture once OGS-side artefacts are accounted for: the residual is linear in ship speed (Pearson $r = +0.67$, linear fit residual $\approx 4.38\,\mathrm{s}\cdot v + 12.95\,\mathrm{m}$, with v in m s^{-1} and residual in metres), which decomposes into a static ≈ 13 m component (reproducing the dwell-only median independently from a disjoint subset of the data, consistent with the physical inter-antenna baseline on the ship's mast) plus a speed-dependent term consistent with an ≈ 4-second lag between the OGS database row-write timestamp and the actual fix epoch. No day in the 149-day overlap exhibits residuals inconsistent with this two-parameter picture. The cross-receiver consistency check therefore confirms that the F9P cruise track contains no anomalies beyond what an L1-only, intermittent reference receiver can itself expose. Absolute precision claims for the F9P are established separately by the within-berth repeatability and the kinematic-PPP residuals (Sect. 5).

[2] Live position and per-campaign historical tracks, https://laurabassi.ogs.it, accessed 2026-05-17. The primary OGS GPS is single-frequency (L1-only) and the historical-track endpoint exposes only {lat, lon, UTC} triples without per-fix quality flags, so OGS-side dropouts and unmodelled-ionosphere bias cannot be filtered out at the matching stage.

https://doi.org/10.5194/essd-2026-432
Preprint. Discussion started: 11 August 2026

Open Access Earth System Science Data Discussions

5.5 Code multipath and cycle slips

Per-arc Estey & Meertens M1/M2 linear combinations (Estey and Meertens, 1999) are computed across the cruise using the dual-band signal pairs natively tracked by the F9P (GPS L1+L5, Galileo E1+E5a, BeiDou B1I+B2a). After per-arc bias removal, the median high-elevation ($\geq 30°$) M1 RMS is 1.04 m at Trieste port (harbour multipath), 0.69 m at the Mario Zucchelli dwell (clear sky), and 0.4 m–0.6 m in mid-Pacific transit (open ocean). Below 30° elevation, M1 RMS rises to 1.5 m–2 m at all latitudes (Fig. 4), consistent with published F9P benchmarks (Hamza et al., 2021). Cycle slips (discontinuities in carrier-phase tracking caused by brief loss of signal lock, a standard GNSS-quality indicator) total 13 221 773 across the cruise, with a mean of ≈ 61 200 per day. A Spearman rank test of daily slip count against absolute geomagnetic latitude (centred-dipole approximation, 2025 epoch) gives $\rho = -0.14$ (nominal $p = 0.035$; the autocorrelation of the daily samples along the cruise track makes nominal p values optimistically small, per Sect. 5.7), too small to be predictive and, more importantly, sign-reversed relative to the physical expectation (the auroral oval drives more slips at higher |B-lat|). The observed weak negative correlation is consistent with an operational-mode confound: high-|B-lat| days are dominated by the Mario Zucchelli anchorage stop, whose calm sky and stationary platform produce the lowest slip rates of the cruise (Fig. 5). Disentangling residual ionospheric signal from operational mode would require a partial correlation controlling for ship state and is left to downstream users.

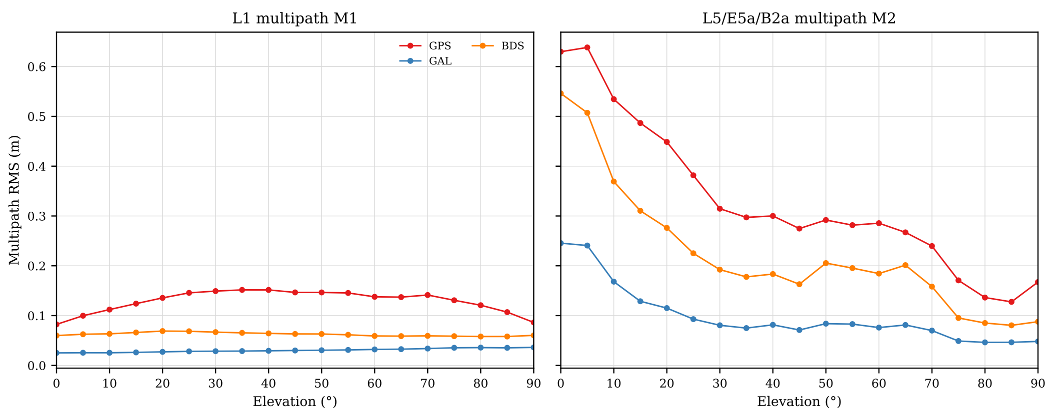

Figure 4. Estey & Meertens code-multipath M1 (left) and M2 (right) RMS versus satellite elevation, per constellation, after per-arc bias removal. Elevations $\geq 30°$ yield sub-metre RMS on open ocean for all dual-band constellations (GPS L1+L5, Galileo E1+E5a, BeiDou B1I+B2a), rising to ≈ 1 m at harbours, consistent with published F9P benchmarks (Hamza et al., 2021).

Daily M1 and M2 root-mean-square values are reported per day together with the cycle-slip count and the slip ratio (slips per 1000 carrier-phase observations), in the Bosser et al. (2021) Table 2 convention. The day-resolved quality-indicator time series (Fig. 5) summarises the slip ratio and M1/M2 RMS across all 216 days of the cruise; the per-day `UBX-NAV-PVT` epoch count is near-constant at the 2 Hz nominal expectation (172 800 epochs day^{-1}) over the continuously-logged days and is not plotted. Three multi-week periods of elevated multipath are visible: the Trieste port stops at either end of the cruise, the Lyttelton port call (centred around mid-November), and the Mario Zucchelli dwell (late January and early February). These

https://doi.org/10.5194/essd-2026-432
Preprint. Discussion started: 11 August 2026

windows coincide with the harbour and anchorage RFI excursions discussed in Sect. 5.7 below. Both signals are consistent with proximity to harbour structures rather than with hardware degradation.

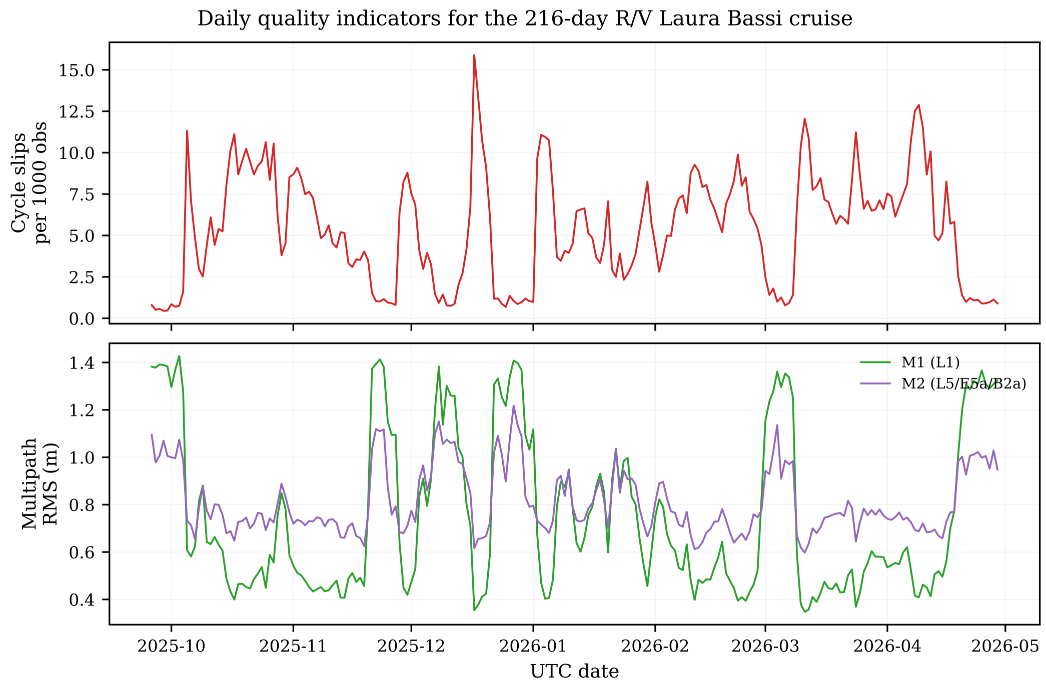

Figure 5. Daily quality indicators across the 216-day cruise. Top panel: cycle-slip ratio (slips per 1000 carrier-phase observations). Bottom panel: code-multipath RMS on the L1 and L5/E5a/B2a bands. The per-day `UBX-NAV-PVT` epoch count is near-constant at the 2 Hz nominal expectation of 172 800 epoch day^{-1} across the continuously-logged days and is therefore not plotted; the per-day totals are tabulated in `T4_daily_stats`. The Lyttelton (mid-November) and Mario Zucchelli (late January–early February) port and anchorage windows are visible as elevated multipath. This is the moving-platform analogue of Männel et al. (2021) Fig. 3.

5.6 Ionospheric product cross-validation against IGS GIM

As a spot-check that the released relative-TEC product (Sect. 4) is consistent with an independent ionospheric reference, we compare the dataset's high-elevation ($\geq 40°$) vertical TEC against the CODE Analysis Centre final Global Ionosphere Map (Hernández-Pajares et al., 2009) on three days chosen to span the cruise's operating modes: a stationary fixed-receiver Trieste pre-departure dock day (2025-09-30), a polar-anchorage high-variability case at Mario Zucchelli (2026-01-27), and an open-ocean mid-Atlantic return-leg day (2026-04-15). This is a sparse spot-check rather than a continuous validation; a fully day-resolved cruise-wide TEC–GIM comparison is left to downstream users. Per-hour median ship-position vTEC is bilinearly interpolated from the $2.5° \times 5°$, 1-hour GIM grid. Because single-receiver geometry-free TEC has an unknown DCB constant,

https://doi.org/10.5194/essd-2026-432
Preprint. Discussion started: 11 August 2026

we subtract a single per-day median offset and report (i) the RMS of the residual (relative agreement) and (ii) the Spearman correlation of the un-offset series (shape agreement, DCB-invariant).

Across the three days the recovered DCB offset is stable (≈ -16 TECU) and the post-offset RMS is a few TECU. The Spearman correlation against GIM is strongest at the fixed-receiver dock ($\rho = +0.96$, 2025-09-30), and remains moderate-to-strong at the more variable sites, $\rho = +0.72$ at the Mario Zucchelli polar anchorage and $\rho = +0.74$ on the mid-Atlantic transit (2026-04-15) (Fig. 6). The lower correlations at the polar-anchorage and open-ocean days are consistent with the higher spatial-temporal variability of those regions relative to the smoothed GIM representation (Alfonsi et al., 2011; Prikryl et al., 2015). The cross-check confirms that the diurnal and large-scale TEC structure recovered by our pipeline tracks the IGS reference. The absolute offset is the unmodelled receiver and satellite DCB constant that downstream users requiring absolute TEC should estimate against external DCB products (e.g., Geng et al. 2022).

5.7 RF spectrum baseline and data-quality variations

The on-board RF spectrum (`UBX-MON-SPAN`) is logged at 1 Hz across the entire cruise, totalling $\approx$18.6 million messages ($\approx$37.3 million per-block spectra, two per message) over the 216-day record (a representative daily waterfall is in Fig. 7). The L1 RF block (centre 1583.5 MHz) shows a low baseline jamming indicator (`UBX-MON-RF.jamInd`) of 17–30 across all sea-going days, with isolated excursions to 60–192 corresponding to port stops and adjacent operations (Table 8). Of the 10 strong-RFI days (defined as L1 `jamInd` peak > 60), eight occur at the Lyttelton (NZ) berth, one at a northbound transit $\approx$90 km from Lyttelton, and one at the Mario Zucchelli anchorage.

Table 8. Strong-RFI days across the 216-day cruise: every UTC day on which the L1 `UBX-MON-RF.jamInd` peak exceeded 60. "lat" and "lon" are the day-median ship position; "speed" is the day-mean ground speed; `L1_max` is the day-peak `jamInd` on the L1 block; `L1 > 60` is the count of epochs with `jamInd` > 60 on the same block.

Day	lat (°)	lon (°)	speed (m/s)	L1_max	L1 > 60
2025-11-23	−43.605	+172.716	0.00	78	4
2025-11-24	−43.605	+172.716	0.00	78	5
2025-12-10	−74.678	+164.161	0.01	126	14
2025-12-22	−43.606	+172.721	0.01	156	14
2025-12-28	−43.605	+172.716	0.00	66	1
2025-12-30	−43.609	+172.731	0.05	82	2
2026-02-28	−44.413	+172.720	4.75	138	441
2026-03-01	−43.606	+172.720	0.01	136	7
2026-03-02	−43.606	+172.720	0.01	134	83
2026-03-08	−43.606	+172.719	0.01	192	12

https://doi.org/10.5194/essd-2026-432
Preprint. Discussion started: 11 August 2026

Open Access Earth System Science Data Discussions

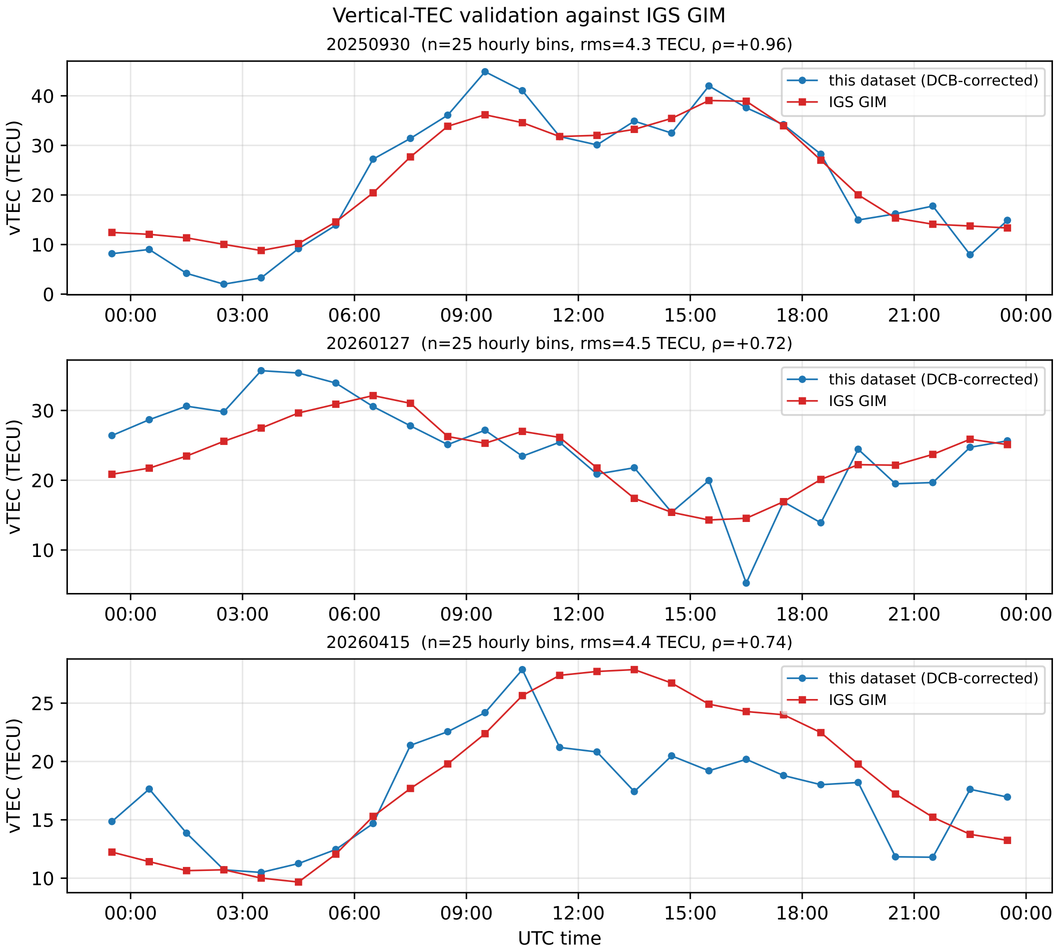

Figure 6. Vertical-TEC cross-validation against the CODE final Global Ionosphere Map on three days spanning the cruise's operating modes. Each panel overlays the dataset's hourly-binned ship-position vTEC (blue, after subtraction of a single per-day median DCB offset) and the GIM bilinearly interpolated at the ship position (red), for a stationary Trieste pre-departure dock day (top, 2025-09-30, $\rho = +0.96$), the Mario Zucchelli polar anchorage (middle, 2026-01-27, $\rho = +0.72$), and a mid-Atlantic return-leg transit (bottom, 2026-04-15, $\rho = +0.74$); the per-panel title reports the number of hourly bins, the post-DCB RMS in TECU, and the Spearman correlation against GIM. The recovered per-day offset is stable at ≈ -16 TECU, the unmodelled receiver-and-satellite DCB.

The L5 RF block carries a higher receiver-internal baseline (`jamInd` 70–100). Unlike the L1 block, this baseline correlates with environmental conditions across the cruise: Spearman $\rho = +0.48$ (nominal $p < 10^{-3}$, $n = 216$ days) against absolute geographic latitude, and Spearman $\rho = -0.32$ (nominal $p < 10^{-3}$) against receiver internal temperature. These two regressors are themselves strongly correlated ($\rho = -0.80$): cold days tend to be high-latitude days. After controlling for receiver temperature, the partial Spearman correlation of `jamInd` on |lat| is $\rho = +0.38$ (nominal $p < 10^{-3}$). After controlling for |lat|, the partial correlation on temperature is $\rho = +0.10$ ($p = 0.14$, not significant) and changes sign relative to the raw correlation.

https://doi.org/10.5194/essd-2026-432
Preprint. Discussion started: 11 August 2026

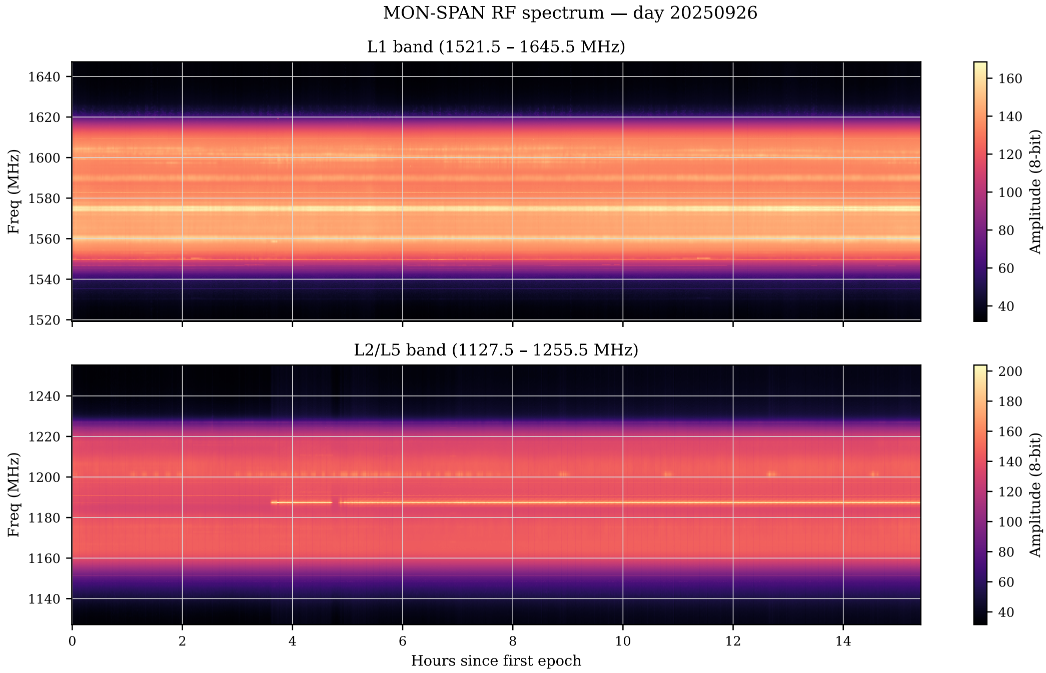

Figure 7. Daily `UBX-MON-SPAN` RF spectrum waterfall on a representative day. Two RF blocks are shown: top, L1 band (centred at 1583.5 MHz, 128 MHz span), and bottom, L5 band (centred at 1191.5 MHz, 128 MHz span). Bright horizontal bands mark the GNSS carriers (GPS L1, GLONASS L1, Galileo E1, GPS L5, Galileo E5a, BeiDou B2a). Vertical features identify per-second spectral excursions logged through the entire cruise.

The nominal p-values quoted here assume independent daily samples and are therefore optimistically small given the auto-correlation of ship-position along the track; the effect sizes (ρ) are the quantities to be relied upon. The apparent temperature dependence is therefore an artefact of the latitude–temperature confound: geographic latitude is the dominant driver of the L5 baseline shift, while internal receiver temperature has no independent effect detectable at the day-aggregated scale. For RFI surveillance on the L5 block we therefore recommend that downstream users compute excursions *relative to a per-day median* rather than against the cruise-wide absolute value, since the absolute `jamInd` value on this block carries a latitude-modulated bias that does not represent only environmental interference. Under the per-day L5 threshold of Table 4, only one day in the cruise records L5 excursions: 2025-12-09 at the Mario Zucchelli anchorage (2 epochs), consistent with the latitude-modulated baseline shift rather than environmental interference.

Per-day RF-spectrum excursion counts (per-bin amplitude above the 5 MAD bin-median threshold, summed over both RF blocks) vary by approximately three orders of magnitude across the cruise. Sub-Antarctic days (latitude $< -60°$, $n = 64$) account for the upper tail (median 3 006 excursions day^{-1}, range 502–122 393).

The multi-signature spoofing detector (Table 5) reports zero cruise days reaching the strong-spoofing threshold $S \geq 5$ on any epoch. Eight days carry epochs above the moderate threshold $S \geq 3$, all at port stops, where the `pos_vel_mismatch`

https://doi.org/10.5194/essd-2026-432
Preprint. Discussion started: 11 August 2026

Open Access Earth System Science Data Discussions

indicator is sensitive to GPS-jitter excursions over a stationary platform and triggers as an artefact of the indicator definition rather than as evidence of spoofing.

5.8 Track-outlier classification

The anomaly catalogue (Sect. 4.3.4) flags 987 epochs across the 216-day cruise. The regional and per-class breakdown is given in Table 9, and the geographic distribution of the L1 strong-RFI episodes is mapped in Fig. 8. The dominant signal is L1 RFI at the Lyttelton mooring (953 of 987 epochs). The only L5 excursions are the 2025-12-09 events at Mario Zucchelli already discussed in Sect. 5.7. Outliers are collapsed to a single class per epoch via a precedence order documented in the released pipeline (spoofing classes outrank RFI, which outrank geometry and cold-start classes).

Table 9. Distribution of flagged outliers by region and collapsed class across the 216-day cruise. Each cell is the count of flagged epochs in the corresponding (region, class) bin. Class precedence is given in Sect. 5.8. The `rfi_l1` and `rfi_l5` columns correspond to the `high_jamming_l1` and `high_jamming_l5` categories of Table 4. Regions where no class populated are omitted. Note: the regional concentration at "mid_southern" reflects the Lyttelton mooring (port-area RFI on the L1 block), consistent with Table 8.

Region	rfi_l5	rfi_l1	no_fix	total
antarctic	2	20	0	22
mediterranean_basin	0	1	9	10
mid_southern	0	953	0	953
tropics	0	2	0	2

6 Limitations and intended-use caveats

- Positioning accuracy is metre-scale, not centimetre-scale. The onboard formal errors are Kalman-filter self-reports known to be optimistic for consumer-grade multi-band receivers on moving platforms (Sect. 5).
- Multi-band coverage is band-asymmetric: the L1L5 firmware variant tracks L1 on every constellation and L5-family signals only on GPS Block IIF/III, Galileo, BeiDou, intermittent QZSS and NavIC; GLONASS, SBAS and legacy GPS are single-band (Sect. 2).
- The L5 RF block's 128 MHz passband (u-blox hardware label "L2/L5") physically extends into the L2 frequency family, so `UBX-MON-SPAN` and `UBX-MON-RF.jamInd` observe both L5 and L2 interference even though only L5-family signals enter the positioning solution (Sect. 2).
- The receiver antenna calibration (marker `TRSAX4E02`, shipped under `rinex3/antex/`) must be merged into the user's IGS20 ATX catalogue when reprocessing. Without this step the receiver-side PCO/PCV corrections silently default to zero (Sect. 4).

https://doi.org/10.5194/essd-2026-432
Preprint. Discussion started: 11 August 2026

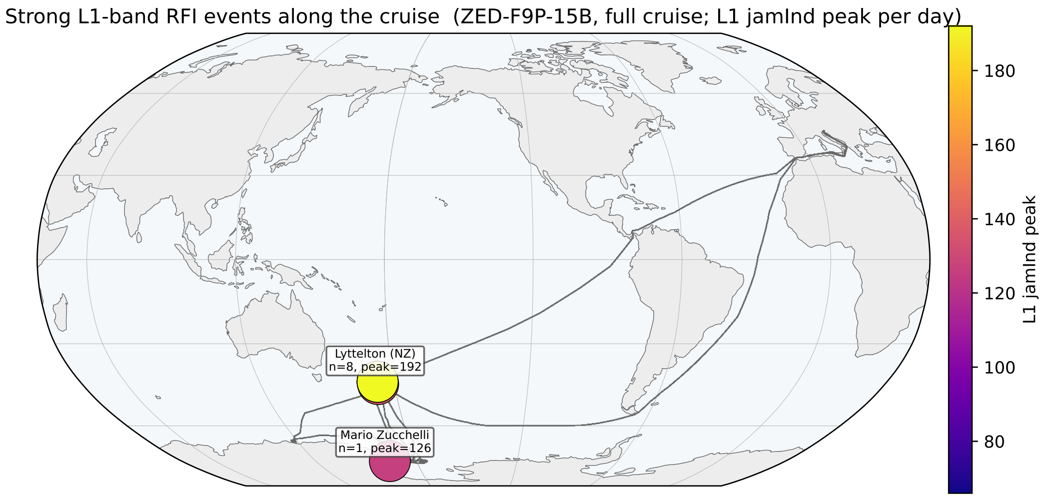

Figure 8. Geographic distribution of strong RFI events along the cruise. "Strong-RFI day" is defined here as any UTC day with at least one `UBX-MON-RF.jamInd` value above 60 on the L1 RF block (the L1 baseline is 17–30 across all sea-going days). The cruise track is overlaid with event markers, each marker placed at the day-median ship position and scaled in size and colour by that day's L1 `jamInd` peak; labelled clusters give the per-site event count and peak `jamInd`. The concentration at Lyttelton (NZ) accounts for the majority of strong-RFI days, with a single Mario Zucchelli excursion.

- The canonical S_4 amplitude scintillation index is not derivable from 2 Hz sampling. We publish a phase-detrended σ_φ proxy and ROTI as relative ionospheric quantities with explicit bandwidth caveats (Sect. 4).
- The L5 jamming-indicator baseline carries a latitude-modulated bias (partial Spearman $\rho = +0.38$ after controlling for receiver temperature, which is itself correlated with latitude). RFI surveillance on this block should use per-day-relative excursions rather than absolute values (Sect. 5.7).
- The firmware version is sourced from the deployment configuration rather than verified from the recorded stream because `UBX-MON-VER` (a poll-on-demand message) was not enabled in the periodic logging configuration (Sect. 3).
- Daily cycle-slip count is a poor day-resolved ionospheric indicator: the weak Spearman correlation against absolute geomagnetic latitude ($\rho = -0.14$, $p = 0.035$) is detectable only because $n = 216$, and the effect size cannot predict individual-day slip rate, which is dominated by operational mode (Sect. 5).

7 Data records

The data archive is released on Zenodo at https://doi.org/10.5281/zenodo.20344101 (Blatnik et al., 2026) under a CC-BY 4.0 licence. Total bundled deposit size is approximately 80 GB. The deposit contains the two primary source products (raw binary and RINEX) together with the metadata needed to interpret them. It is organised under three top-level directories. `raw/` holds

https://doi.org/10.5194/essd-2026-432
Preprint. Discussion started: 11 August 2026

Open Access Earth System Science Data Discussions

the 216 daily `.ubx` files (176.9 GB uncompressed) packaged as eight 7z monthly archives (`ubx_YYYY_MM.7z`, 63.4 GB total); two days within the deposit are partial: 2025-09-26 (receiver power-up at the dock) and 2026-04-29 (return arrival). `rinex3/` holds the Hatanaka-compressed RINEX 3.04 OBS+NAV re-distribution (≈17 GB) in the long IGS file-naming convention, with the NGS-calibrated AX4E02 ATX under `rinex3/antex/`. `metadata/` holds the IGS-style site log, a deposit `README` documenting layout and provenance, and a machine-readable manifest (`metadata/checksums.sha256`) providing SHA-256 checksums for every file. The associated processing code is bundled in the same Zenodo deposit alongside the data (`code/` subtree; Sect. 10). Selected cruise-wide quality metrics computed by the pipeline are summarised in Table 10.

Table 10. Selected quality metrics summary across the 216-day cruise. Within-berth repeatability is the standard deviation of median ship position across multiple stationary visits to the same physical berth (10 berths with $n \geq 3$ visits, greedy 50 m sub-clustering on the per-visit median position).

Metric	Value
Receiver internal consistency, 2-D 95 %	6 mm
Within-berth repeatability, cross-cluster median ($n_{\text{berth}} = 10$)	0.57 m
Within-berth repeatability, best (Trieste return pier, $n = 10$)	0.115 m
At-anchorage repeatability (Mario Zucchelli, $n = 20$)	1.24 m
Code multipath M1, high-elev port	1.04 m
Code multipath M1, high-elev Antarctic dwell	0.69 m
Code multipath M1, high-elev mid-ocean	0.4 m–0.6 m
Receiver fix availability across 216 days	100.00 %
Days with spoofing-suspicion score $\geq 5/7$	0

8 Comparison with prior shipborne campaigns

The closest comparable openly-released shipborne GNSS datasets are listed in Table 11. The most directly comparable is our own single-frequency predecessor from the same vessel (Bertalanič et al., 2026): the present campaign is an independent acquisition over a different polar mission (2025–2026 rather than 2024–2025), recorded with a dual-band u-blox ZED-F9P-15B in place of the single-frequency MAX-M10S. The upgrade is not merely an additional band: the L5/E5a/B2a observables enable dual-frequency ionosphere-free positioning, geometry-free TEC and ROTI products, and kinematic PPP cross-validation that are not derivable from a single-frequency record, and the second RF block extends RFI surveillance across the L5/L2 passband. The present dataset is therefore a new acquisition with capabilities the earlier record did not have, rather than a re-release or re-processing of it. The present record extends prior work along three independent axes: (i) it preserves raw observables on the modernised L5/E5a/B2a civil band in addition to L1, where prior shipborne ESSD releases used L1/L2 only; (ii) within the structured survey documented in Sect. 1 we found no prior multi-month shipborne record preserving *dual-RF-block* on-board `UBX-MON-SPAN` radio-frequency spectrum spanning both the L1 and L5 receiver blocks, extending the L1-only preservation

Table 11. Comparison of the present dataset with the closest openly released *shipborne* GNSS datasets. "Bands" lists the carrier frequencies preserved in the raw observable stream. "Spectrum" indicates whether the on-board receiver RF spectrum (`UBX-MON-SPAN` or equivalent) is preserved alongside the raw observables, and over which receiver RF blocks. "This dataset" refers to the campaign described in the present paper. Fixed-network multi-year datasets such as the Antarctic bedrock GNSS reprocessing (Buchta et al., 2025) and the IGS climate data record (Wang et al., 2025) are cited in the text for methodological context but are not platform-comparable and are omitted from this table.

Dataset	Duration	Receiver	Constellations / Bands	Spectrum	Latitudinal range
This dataset (this paper)	216 d	u-blox ZED-F9P-15B	GPS, GLO, GAL, BDS, SBAS, QZSS, NavIC L1, L5/E5a/B2a	L1 + L5 blocks	45.6° N to 74.8° S
Antarctic L1 (Bertalanič et al., 2026)	200 d	u-blox MAX-M10S	GPS, GLO, GAL, BDS (L1 only) L1	L1 block only	45.6° N to 74.7° S
EUREC4A (Bosser et al., 2021)	∼40 d	Septentrio PolaRx5	GPS, GLO, GAL, BDS L1, L2	no	Tropical Atlantic only
MOSAiC (Männel et al., 2021)	12 mo (drift)	Trimble NetR9	GPS, GLO, GAL L1, L2	no	79° N–88° N (drifting)
MAP-IO (Tulet et al., 2024)	multi-year	geodetic (multi-instrument)	GPS, GLO, GAL, BDS L1, L2	no	Indian + Southern Ocean

of our prior single-frequency release (Bertalanič et al., 2026); and (iii) it samples ≈120° of geographic latitude including eight crossings of the Antarctic Circle, an itinerary not covered by EUREC4A, MOSAiC or any other openly released GNSS dataset listed in Table 11.

9 Conclusions

The dataset combines multi-band carrier-phase observables with the on-board dual-RF-block radio-frequency spectrum (`UBX-MON-SPAN`) across a 216-day round-trip Antarctic voyage spanning ≈120° of latitude. Quality assessment over the full record finds a 3-D fix on every epoch after cold-start, sub-metre code multipath at elevations above 30° on open ocean, decimetre-to-metre within-berth horizontal repeatability, no strong-spoofing days, and one substantive geographic finding: Lyttelton (NZ) and its approaches are a concentrated L-band RFI hotspot (nine of ten cruise-wide strong-RFI days). Intended downstream uses span kinematic positioning, tropospheric water-vapour and relative ionospheric (TEC, ROTI, σ_φ proxy) products, and shipborne L-band RFI surveillance, with bandwidth limits and configuration caveats documented in Sect. 6.

10 Code availability

The full processing pipeline used to produce every artefact in this dataset is available as an open-source Python package under the MIT licence. A frozen snapshot tagged `v1.0` corresponding to the released dataset is bundled inside the same Zenodo deposit as the data under the `code/` subtree (https://doi.org/10.5281/zenodo.20344101, Blatnik et al., 2026). The development repository is mirrored on GitHub at https://github.com/sensorlab/AntarcticaData.

https://doi.org/10.5194/essd-2026-432
Preprint. Discussion started: 11 August 2026

The data deposit bundles the raw `.ubx` files and the RINEX 3.04 set. Every other artefact referenced in this paper (per-message Apache Parquet tables, the `UBX-MON-SPAN` Zarr v3 store, the cruise-track NetCDF and GeoJSON, the per-day anomaly and spoofing catalogues, the cruise-wide quality-control tables, the kinematic PPP outputs, the residual figures of this paper) is reproduced deterministically from the raw `.ubx` files by this pipeline. The Python parsing, derived-analysis and figure-rendering stages require Python $\geq$ 3.11 with the dependencies pinned in `pyproject.toml`. The command `snakemake --cores N stage_parse stage_derive stage_render` regenerates this set in about one wall hour on a 32-core workstation. Reproducing the RINEX 3.04 archive itself (provenance check) and the kinematic-PPP derived products requires two additional external tools not installable via pip: `convbin` (RTKLIB demo5 fork, built from the C sources distributed by Everett (2024)) and `pdp3` (PRIDE PPP-AR (Geng et al., 2024), built from the Fortran sources distributed by Wuhan University at https://github.com/PrideLab/PRIDE-PPPAR). The release ships build scripts under `code/external/` that fetch and compile both on a standard Linux toolchain (`gcc`/`gfortran`, `make`, `bc`). The full RINEX + PPP stage adds approximately three wall hours on the same 32-core workstation.

11 Data availability

The complete dataset described in this paper is archived on Zenodo: https://doi.org/10.5281/zenodo.20344101 (Blatnik et al., 2026). The deposit is publicly accessible under open access with a resolving DOI. No login, registration or access request is required. The full GNSS record is released openly under CC-BY 4.0 for every cruise segment. No portion was withheld, downsampled or redacted to satisfy any coastal-state or treaty constraint.

Author contributions. B.B. led the data-pipeline development and analysis, contributed to the design of the recording chain, and drafted the manuscript. F.D. provided the maritime expertise, and supported deployment. A.B. designed the recording chain and led the field deployment on R/V *Laura Bassi*. All authors contributed to the manuscript writing, reviewing, and editing.

Competing interests. The authors declare no competing interests.

Acknowledgements. We thank the Istituto Nazionale di Oceanografia e di Geofisica Sperimentale (OGS) and the captain and crew of R/V *Laura Bassi* for hosting the recording installation. This work was supported by the Slovenian Research and Innovation Agency (ARIS) through research programme P2-0016 (Communication Networks and Services), research project L7-60164 (Sustainable and Digital Framework for Safety and Protection in Ports).

https://doi.org/10.5194/essd-2026-432
Preprint. Discussion started: 11 August 2026

Open Access Earth System Science Data Discussions

References

Alfonsi, L., Spogli, L., De Franceschi, G., Romano, V., Aquino, M., Dodson, A., and Mitchell, C. N.: Bipolar climatology of GPS ionospheric scintillation at solar minimum, Radio Science, 46, https://doi.org/10.1029/2010RS004571, 2011.

Bertalanič, B., Dimc, F., Bažec, M., and Blatnik, A.: Voyage to the Frozen Continent: A Comprehensive GNSS Dataset from a Ship's Expedition to Antarctica, Scientific Data, 13, 49, https://doi.org/10.1038/s41597-025-06366-x, 2026.

Bevis, M., Kendrick, E., Smalley, R., Dalziel, I., Caccamise, D., Sasgen, I., Helsen, M., et al.: Geodetic measurements of vertical crustal velocity in West Antarctica and the implications for ice mass balance, Geochemistry, Geophysics, Geosystems, 10, https://doi.org/10.1029/2009GC002642, 2009.

Blatnik, A., Bertalanič, B., and Dimc, F.: A Comprehensive GNSS Dataset from the 41st Laura Bassi Expedition to Antarctica, https://doi.org/10.5281/zenodo.20344101, [data set], 2026.

Borio, D. and Gioia, C.: Real-time jamming detection using the sum-of-squares paradigm, in: 2015 International Conference on Location and GNSS (ICL-GNSS), pp. 1–6, https://doi.org/10.1109/ICL-GNSS.2015.7217161, 2015.

Bosser, P., Bock, O., Flamant, C., Bony, S., and Speich, S.: Integrated water vapour content retrievals from ship-borne GNSS receivers during EUREC4A, Earth System Science Data, 13, 1499–1517, https://doi.org/10.5194/essd-13-1499-2021, 2021.

Buchta, E., Scheinert, M., King, M. A., Wilson, T., Koulali, A., Clarke, P. J., Gómez, D., et al.: Advancing geodynamic research in Antarctica: reprocessing GNSS data to infer consistent coordinate time series (GIANT-REGAIN), Earth System Science Data, 17, 1761–1780, https://doi.org/10.5194/essd-17-1761-2025, 2025.

Dovis, F., ed.: GNSS Interference, Threats, and Countermeasures, Artech House, ISBN 978-1-60807-810-3, 2015.

Estey, L. H. and Meertens, C. M.: TEQC: the multi-purpose toolkit for GPS/GLONASS data, GPS Solutions, 3, 42–49, https://doi.org/10.1007/PL00012778, 1999.

Everett, T. r.: RTKLIB demo5 fork: post-processing of low-cost GNSS receivers, https://github.com/rtklibexplorer/RTKLIB, 2024.

Geng, J., Zhang, Q., Li, G., Liu, J., and Liu, D.: Observable-specific phase biases of Wuhan multi-GNSS experiment analysis center's rapid satellite products, Satellite Navigation, 3, 23, https://doi.org/10.1186/s43020-022-00084-0, 2022.

Geng, J., Zhang, H., Li, G., and Aoki, Y.: Multipath mitigation for GPS/Galileo/BDS-3 precise point positioning with overlap-frequency signals, Satellite Navigation, 5, 22, https://doi.org/10.1186/s43020-024-00144-7, 2024.

Hamza, V., Stopar, B., and Sterle, O.: Testing the Performance of Multi-Frequency Low-Cost GNSS Receivers and Antennas, Sensors, 21, 2029, https://doi.org/10.3390/s21062029, 2021.

Hernández-Pajares, M., Juan, J. M., Sanz, J., Orus, R., Garcia-Rigo, A., Feltens, J., Komjathy, A., Schaer, S. C., and Krankowski, A.: The IGS VTEC maps: a reliable source of ionospheric information since 1998, Journal of Geodesy, 83, 263–275, https://doi.org/10.1007/s00190-008-0266-1, 2009.

Jakowski, N., Beniguel, Y., De Franceschi, G., et al.: Monitoring, tracking and forecasting ionospheric perturbations using GNSS techniques, Journal of Space Weather and Space Climate, 2, https://doi.org/10.1051/swsc/2012022, 2012.

Krietemeyer, A., van der Marel, H., van de Giesen, N., and ten Veldhuis, M. C.: High Quality Zenith Tropospheric Delay Estimation Using a Low-Cost Dual-Frequency Receiver and Relative Antenna Calibration, Remote Sensing, 12, https://doi.org/10.3390/rs12091393, 2020.

Männel, B., Zus, F., Dick, G., Glaser, S., Semmling, M., Balidakis, K., Wickert, J., Maturilli, M., Dahlke, S., and Schuh, H.: GNSS-based water vapor estimation and validation during the MOSAiC expedition, Atmospheric Measurement Techniques, 14, 5127–5138, https://doi.org/10.5194/amt-14-5127-2021, 2021.

Montenbruck, O., Steigenberger, P., Prange, L., Deng, Z., Zhao, Q., Perosanz, F., Romero, I., Noll, C., Stürze, A., Weber, G., Schmid, R., MacLeod, K., and Schaer, S.: The Multi-GNSS Experiment (MGEX) of the International GNSS Service (IGS) – achievements, prospects and challenges, Advances in Space Research, 59, https://doi.org/10.1016/j.asr.2017.01.011, 2017.

Morrison, A., Sokolova, N., and Ahmed, N.: RFI Monitoring in Support of Safety-Critical Multi-Band GNSS-based Systems, in: 2019 European Navigation Conference (ENC), pp. 1–6, https://doi.org/10.1109/EURONAV.2019.8714133, 2019.

Negusini, M., Petkov, B. H., Tornatore, V., Barindelli, S., Martelli, L., Sarti, P., and Tomasi, C.: Water Vapour Assessment Using GNSS and Radiosondes over Polar Regions and Estimation of Climatological Trends from Long-Term Time Series Analysis, Remote Sensing, 13, 4871, https://doi.org/10.3390/rs13234871, 2021.

NOAA National Geodetic Survey: Antenna Calibration Database (ANTCAL), https://geodesy.noaa.gov/ANTCAL/, 2026.

NOAA Space Weather Prediction Center: Solar Cycle 25 Progression, https://www.swpc.noaa.gov/products/solar-cycle-progression, accessed 2026-05-08, 2026.

Pi, X., Mannucci, A. J., Lindqwister, U. J., and Ho, C. M.: Monitoring of global ionospheric irregularities using the worldwide GPS network, Geophysical Research Letters, 24, https://doi.org/10.1029/97GL02273, 1997.

Poluzzi, L., Tavasci, L., Corsini, F., Barbarella, M., and Gandolfi, S.: Low-cost GNSS sensors for monitoring applications, Applied Geomatics, 12, https://doi.org/10.1007/s12518-019-00268-5, 2020.

Prikryl, P., Jayachandran, P. T., Chadwick, R., and Kelly, T. D.: Climatology of GPS phase scintillation at northern high latitudes for the period from 2008 to 2013, Annales Geophysicae, 33, https://doi.org/10.5194/angeo-33-531-2015, 2015.

Tersus GNSS Inc.: AX4E02 Full-Constellation Survey Antenna Datasheet, Version V1.4-20241028, https://www.tersus-gnss.com/product/antenna-ax4E02, 2024.

Tulet, P., Van Baelen, J., Bosser, P., Brioude, J., Colomb, A., Goloub, P., Pazmino, A., et al.: MAP-IO: an atmospheric and marine observatory programme onboard Marion Dufresne over the Southern Ocean and Indian Ocean, Earth System Science Data, 16, 3821–3849, https://doi.org/10.5194/essd-16-3821-2024, 2024.

u-blox AG: ZED-F9P-15B High Precision GNSS Module Data Sheet, Document UBX-23009090, https://www.u-blox.com/en/product/zed-f9p-module, 2024.

Wang, X., Li, H., Choy, S., Huang, Q., Cai, W., Rea, A., Zhang, H., et al.: A global GNSS climate data record from 5085 stations spanning up to 22 years, Earth System Science Data, 17, 5951–5982, https://doi.org/10.5194/essd-17-5951-2025, 2025.

Wuhan University IGS Analysis Center: Wuhan University Multi-GNSS Rapid (WUM) precise orbit, clock, attitude, ERP and observable-specific code/phase-bias products, Available via FTPS: ftps://bdspride.com/wum/; product line description at the Wuhan Combination Center page, https://igs.org/wg/wcc/, multi-GNSS Experiment (MGEX) Analysis Center products `WUM0MGXRAP_*`: 5-min orbits, 30-s clocks, 30-s attitude quaternions, daily ERP and observable-specific biases for GPS, GLONASS, Galileo, BeiDou and QZSS, 2024.